ISSN 2071-2898 (Print)
ISSN 2071-2901 (Online)

Rogov B.V.

Dispersive and dissipative properties of the fully discrete bicompact schemes of the fourth order of spatial approximation for hyperbolic equations

Recommended form of bibliographic references: Rogov B.V. Dispersive and dissipative properties of the fully discrete bicompact schemes of the fourth order of spatial approximation for hyperbolic equations // Keldysh Institute Preprints. 2018. No. 153. 30 p. doi:10.20948/prepr-2018-153-e
URL: http://library.keldysh.ru/preprint.asp?id=2018-153&lg=e

KELDYSH INSTITUTE OF APPLIED MATHEMATICS

R u s s i a n A c a d e m y o f S c i e n c e s

B.V.Rogov

Dispersive and dissipative properties of the fully discrete bicompact schemes of the fourth order of spatial approximation for hyperbolic equations

Moscow — 2018

Boris Vadimovich Rogov

Dispersive and dissipative properties of the fully discrete bicompact schemes of the fourth order of spatial approximation for hyperbolic equations

The Fourier analysis of fully discrete bicompact fourth-order spatial approximation schemes for hyperbolic equations is presented. This analysis is carried out on the example of a model linear advection equation. The results of Fourier analysis are presented as graphs of the dependence of the dispersion and dissipative characteristics of the bicompact schemes on the dimensionless wave number and the Courant number. The dispersion and dissipative properties of bicompact schemes are compared with those of other widely used difference schemes for hyperbolic equations. It is shown that bicompact schemes have one of the best spectral resolutions among the difference schemes being compared.

Keywords: hyperbolic equations, bicompact schemes, dispersion, dissipation

Рогов Б.В.

Дисперсионные и диссипативные свойства полностью дискретных бикомпактных схем четвертого порядка пространственной аппроксимации для уравнений гиперболического типа

Представлен Фурье-анализ полностью дискретных бикомпактных схем четвертого порядка пространственной аппроксимации для уравнений гиперболического типа. Такой анализ проведен на примере модельного линейного уравнения переноса. Результаты Фурье-анализа представлены в виде графиков зависимости дисперсионных и диссипативных характеристик бикомпактных схем от безразмерного волнового числа и числа Куранта. Проведено сравнение дисперсионных и диссипативных свойств бикомпактных схем с аналогичными свойствами других широко используемых разностных схем для уравнений гиперболического типа. Показано, что бикомпактные схемы имеют одно из лучших спектральных разрешений среди сравниваемых разностных схем.

Ключевые слова: уравнения гиперболического типа, бикомпактные схемы, дисперсия, диссипация

This research was supported by the Russian Foundation for Basic Research, project 18-01-00857-a.

1. Introduction

Numerical modeling of long-time and long-distance propagation of acoustic, electromagnetic, and elastic waves requires schemes that have low dissipation and low dispersion. Widely used symmetric compact schemes possess such properties. Moreover, these schemes have superior spectral resolution compared to classic symmetric finite difference schemes of the same order of accuracy [1-3]. However, the spatial stencil of well-known symmetric compact schemes contains no less than three integer nodes in each space dimension, therefore, these schemes can be used for computations only on uniform or weakly non-uniform meshes [1, 4, 5].

The semi-discrete bicompact scheme of the fourth order of approximation in space was proposed in [6] for numerical solution of quasilinear one-dimensional advection equation. The semi-discrete bicompact scheme is constructed by method of lines on the spatial stencil that fits one mesh cell and contains two integer and one half-integer node. The number of differential-difference equations of the semi-discrete scheme equals two, thus its effective difference order, defined as the difference between the total number of stencil nodes and the number of scheme equations, equals one and matches the order of the differential advection equation with respect to space variable. As a result of the orders equality, differential and numerical problems have the same number of boundary conditions. In addition, in case of advection speed of fixed sign the semi-discrete scheme can be solved using the space marching method [6]. The high order of approximation of the bicompact schemes remains the same even on strongly non-uniform meshes which is guaranteed by the construction. Equations of the semi-discrete scheme are proposed to be integrated in time by multi-stage A- and L-stable diagonally implicit Runge-Kutta (RK) methods that are numerically efficient in comparison with fully implicit RK [7]. The scheme [6] was generalized for systems of equations and many space dimensions in [8-10].

The semi-discrete symmetric bicompact scheme [6] is non-dissipative. Its dispersion analysis was done in [11]. In present work, we perform a Fourier analysis of the two fully discrete bicompact schemes, one of them is dissipative and the other is non-dissipative. These two-layer schemes are obtained by implementing the implicit Euler method and the trapezoid rule [7] to the semi-discrete scheme for time integration. Both of these schemes consist of two difference equations for values of the sought mesh function in integer and half-integer nodes. Prior to the Fourier analysis, these two-layer bicompact difference schemes are transformed into three-layer schemes, each consisting of one difference equation for values of the sought mesh function in integer nodes only. Dispersion and dissipation characteristics of the considered bicompact schemes are compared to those of well-known numerical schemes for hyperbolic equations.

2. Semi-discrete symmetric bicompact scheme

Consider the scalar one-dimensional quasilinear advection equation:

$$L_1 u \equiv \frac{\partial u}{\partial t} + \frac{\partial f(u)}{\partial x} = 0, \; \frac{df(u)}{du} > 0. \tag{1}$$

The first equation of the semi-discrete bicompact scheme [6] of the fourth order of approximation in x is obtained by integrating Eq. (1) along the cell $[x_j, x_{j+1}]$ of a non-uniform spatial mesh and by implementing the Simpson's rule:

$$\frac{h_{j+1/2}}{6}\frac{d}{dt}\left(u_{j+1} + 4u_{j+1/2} + u_j\right) + f_{j+1} - f_j = 0, \; f_j = f(u_j), \tag{2}$$

where the spatial step $h_{j+1/2} = x_{j+1} - x_j$. The second equation of the scheme [6]

$$\frac{h_{j+1/2}}{4}\frac{d}{dt}\left(u_{j+1} - u_j\right) + f_{j+1} - 2f_{j+1/2} + f_j = 0, \; f_{j+1/2} = f(u_{j+1/2}) \tag{3}$$

is obtained by the finite difference approximation of the equation

$$(L_1 u)_{j+1} - (L_1 u)_j = 0 \tag{4}$$

which may be regarded as the result of integrating the differential consequence $\partial(L_1 u)/\partial x = 0$ of Eq. (1) along the cell $[x_j, x_{j+1}]$.

Since further calculations are done for the cell $[x_j, x_{j+1}]$ only, let us omit index of the step $h_{j+1/2}$ for brevity.

System of Eqs. (2), (3) may be derived in another way. In order to do this, let us rewrite Eq. (1) in the following form:

$$\frac{\partial f(u)}{\partial x} = \psi(x, u), \tag{5}$$

where

$$\psi = -\frac{\partial u}{\partial t}. \tag{6}$$

To integrate Eq. (5) with respect to x at the time level $t = const$ one may use the Lobatto IIIA scheme (for instance, see [7]) which is a fully implicit stiffly accurate fourth order RK method of collocation type. Its Butcher's table is

$$
\begin{array}{c|ccc}
0 & 0 & 0 & 0 \\
\frac{1}{2} & \frac{5}{24} & \frac{1}{3} & -\frac{1}{24} \\
1 & \frac{1}{6} & \frac{2}{3} & \frac{1}{6} \\
\hline
 & \frac{1}{6} & \frac{2}{3} & \frac{1}{6}
\end{array}.
$$

The Lobatto IIIA integration along $[x_j, x_{j+1}]$ yields a system of two difference equations:

$$f_{j+1} = f_j + \frac{h}{6}\left(\psi_j + 4\psi_{j+1/2} + \psi_{j+1}\right), \tag{7}$$

$$f_{j+1/2} = f_j + \frac{h}{24}\left(5\psi_j + 8\psi_{j+1/2} - \psi_{j+1}\right), \tag{8}$$

where $\psi_j = \psi(x_j, u_j), \psi_{j+1/2} = \psi(x_{j+1/2}, u_{j+1/2})$. Note that the Lobatto IIIA scheme is A-stable and, therefore, absolute stable. Its stencil includes two integer nodes and one half-integer node that are also nodes of the Simpson's quadrature which, in turn, is a special case of the Lobatto quadrature [7].

Next, Eq. (8) is replaced by the linear combination of Eqs. (7) and (8):

$$f_{j+1} - 2f_{j+1/2} = -f_j - \frac{h}{4}\left(\psi_{j+1} - \psi_j\right) \tag{9}$$

which is obtained by subtracting the doubled Eq. (8) from Eq. (7). Finally, substitution of Eq. (6) into Eqs. (7) and (9) transforms them into Eqs. (2) and (3) respectively.

Practically, the Lobatto IIIA scheme for numerical integration of Eq. (1) along discrete variable x is incorporated into the semi-discrete implicit bicompact scheme of the fourth order of approximation in space.

In the case of the linear advection equation

$$\frac{\partial u}{\partial t} + c\frac{\partial u}{\partial x} = 0, \;\; c = const > 0 \tag{10}$$

the semi-discrete bicompact scheme (2), (3) is written as

$$\frac{h}{6c}\frac{d}{dt}\left(u_{j+1}+4U_{j+1/2}+u_j\right)+u_{j+1}-u_j=0,$$
$$\frac{h}{4c}\frac{d}{dt}\left(u_{j+1}-u_j\right)+u_{j+1}-2U_{j+1/2}+u_j=0 \tag{11}$$

where $U_{j+1/2}(t)\equiv u_{j+1/2}(t)$. Eq. (11) may be considered as a system of equations for two time-dependent mesh functions. One of them, $u_j(t)$, is defined on the set of integer nodes and the other, $U_{j+1/2}(t)$, is defined on the set of half-integer nodes [11]. The function $u_j(t)$ may be counted as the main function, while the function $U_{j+1/2}(t)$ takes a role of an auxiliary function which makes it possible for the scheme (11) to have the fourth order of approximation in *x* on the minimal spatial stencil consisting of two integer nodes.

In conclusion to this section let us point out that the semi-discrete bicompact scheme (2), (3) for Eq. (1) is “nonstandard” in some sense.

From Eq. (1) we have

$$\frac{\partial u}{\partial t}=-\frac{\partial f(u)}{\partial x}. \tag{12}$$

Let us formally replace time derivatives by space derivatives in Eqs. (2), (3) according to the formula (12). As a result, we obtain

$$\frac{1}{6}f'_j+\frac{2}{3}f'_{j+1/2}+\frac{1}{6}f'_{j+1}=\frac{1}{h}\left(f_{j+1}-f_j\right), \tag{13}$$

$$\frac{1}{4}f'_{j+1}-\frac{1}{4}f'_j=\frac{1}{h}\left(f_{j+1}-2f_{j+1/2}-f_j\right), \tag{14}$$

where $f'\equiv\partial f/\partial x$. Eqs. (13) and (14) may be interpreted as approximate relations introduced by Eqs. (2) and (3) that connect values of the function f and values of its derivative f' on the mesh. Clearly, these two relations are different, and none of them may be obtained from the other one by shifting all indices by the same number, for example, by 1/2.

To understand how the semi-discrete bicompact scheme (2), (3) is “nonstandard”, let us compare it with a semi-discrete compact scheme of the fourth order of approximation in space from [12]. This scheme, just like the bicompact one, consists of two differential-difference equations

$$\frac{1}{24}\frac{d}{dt}\left(u_{j-1}+22u_j+u_{j+1}\right)+\frac{1}{h}(f_{j+1/2}-f_{j-1/2})=0, \tag{15}$$

$$\frac{1}{24}\frac{d}{dt}\left(u_{j-3/2}+22u_{j-1/2}+u_{j+1/2}\right)+\frac{1}{h}(f_j-f_{j-1})=0 \tag{16}$$

on the uniform spatial mesh with the step $h=x_{j+1}-x_j=x_{j+1/2}-x_{j-1/2}$. The stencil of the scheme (15), (16) includes three integer and three half-integer nodes, while the stencil of the bicompact scheme (2), (3) includes two integer and one half-integer nodes. Substitution of Eq. (12) into Eqs. (15), (16) yields approximate relations between f and f' values at stencil nodes:

$$\frac{1}{24}f'_{j-1}+\frac{11}{12}f'_j+\frac{1}{24}f'_{j+1}=\frac{1}{h}\left(f_{j+1/2}-f_{j-1/2}\right), \tag{17}$$

$$\frac{1}{24}f'_{j-3/2}+\frac{11}{12}f'_{j-1/2}+\frac{1}{24}f'_{j+1/2}=\frac{1}{h}\left(f_j-f_{j-1}\right). \tag{18}$$

Eq. (17) turns into Eq. (18) if the index j is shifted by 1/2.

3. Dispersive properties of semi-discrete bicompact schemes

Semi-discrete bicompact schemes of even orders of approximation in space are constructed upon symmetric spatial stencil [6, 13, 14], they are symmetric and non-dissipative. Dispersive properties of the fourth order accurate semi-discrete bicompact scheme were investigated in [11], similar properties of higher order semi-discrete bicompact schemes were studied in [13, 14]. The optimized semi-discrete symmetric bicompact scheme of the sixth order of approximation was found in [15], its numerical group velocity is least divergent from the exact group velocity. In present work, the expression for numerical (modified, effective) wavenumber of the fourth order accurate semi-discrete bicompact scheme is obtained using the technique from [16].

Consider the linear advection equation (10) on the whole x axis. Assume its solution is a harmonic with the real wavenumber k:

$$u(x,t)=f(t)e^{ikx}, \tag{19}$$

where i is imaginary unit and the function $f(t)$ (amplitude) satisfies the ordinary differential equation (ODE)

$$df/dt=-ickf. \tag{20}$$

If the spatial derivative in Eq. (10) is approximated by a finite difference formula, then Eq. (20) is replaced by the following ODE [16]:

$$df/dt = -ick^* f\,, \tag{21}$$

where k^* is the numerical (modified, effective) wavenumber. Integration of Eq. (21) yields the general solution for the function f:

$$f(t) = Ce^{-ick^* t}\,, \tag{22}$$

where C is an arbitrary constant. The solution of the semi-discrete finite difference scheme corresponding to the function (22) takes the following form at nodes $x = x_j$:

$$u_j(t) = Ce^{-ick^* t} e^{ikx_j}\,. \tag{23}$$

Let us find the numerical wavenumber for the semi-discrete bicompact scheme consisting of two coupled equations (11). It is natural to presume that the nontrivial solution $u_j(t)$ and $U_{j+1/2}(t)$ of Eq. (11) has the form similar to (23):

$$u_j(t) = C_1 e^{-ick^* t} e^{ikx_j},\ U_{j+1/2}(t) = C_2 e^{-ick^* t} e^{ikx_{j+1/2}},\ C_1 = const,\ C_2 = const\,, \tag{24}$$

where

$$C_1^2 + C_2^2 > 0\,. \tag{25}$$

By substituting functions (24) into Eq. (11) we derive the system of two homogeneous linear algebraic equations for coefficients C_1 and C_2:

$$\begin{aligned}
&\left[\sin\left(\frac{1}{2}\varphi\right) - \frac{1}{6}\varphi^* \cos\left(\frac{1}{2}\varphi\right)\right] C_1 - \frac{1}{3}\varphi^* C_2 = 0,\\
&\left[\frac{1}{4}\varphi^* \sin\left(\frac{1}{2}\varphi\right) + \cos\left(\frac{1}{2}\varphi\right)\right] C_1 - C_2 = 0,
\end{aligned} \tag{26}$$

where $\varphi = kh$ and $\varphi^* = k^* h$ are the exact (physical) and the numerical dimensionless wavenumbers respectively. The system of linear algebraic equations (26) has a nontrivial solution satisfying Eq. (25) if the system determinant equals zero. This equality leads to the following relation between quantities φ and φ^*:

$$(\varphi^*)^2 + 6\cot(0.5\varphi)\varphi^* - 12 = 0\,. \tag{27}$$

Earlier, this relation was obtained in [11]. Note that Eq. (27) is quadratic with respect to φ^*, and its discriminant is positive. Therefore, Eq. (27) has only real solutions, i.e. $\mathrm{Im}(k^*)=0$. It means that the semi-discrete bicompact scheme is non-dissipative. Let us remind that this property is common for symmetric semi-discrete schemes.

If $\mathrm{Im}(k^*)=0$, then the numerical wavenumber k^* is related to the numerical phase velocity c^* by the following formula [16]:

$$\frac{c^*}{c}=\frac{k^*}{k}. \tag{28}$$

The relation (28) together with Eq. (27) defines c^* as a function of the wavenumber k in case of the bicompact scheme (2), (3), i.e. they describe dispersive properties of this scheme.

From Eq. (27) we obtain the explicit formula for φ in dependence of φ^*:

$$\varphi = 2\arctan\left(\frac{6\varphi^*}{12-(\varphi^*)^2}\right). \tag{29}$$

The curve described by Eq. (29) goes through the point (0,0) on the (φ,φ^*) plane. Inverting this dependency in the area $\varphi\in[0,\pi]$ yields the formula [11]:

$$\varphi^* = 3\left[\sqrt{\cot^2\left(\frac{\varphi}{2}\right)+\frac{4}{3}}-\cot\left(\frac{\varphi}{2}\right)\right]=\frac{4\tan\left(\frac{\varphi}{2}\right)}{1+\sqrt{1+\frac{4}{3}\tan^2\left(\frac{\varphi}{2}\right)}}. \tag{30}$$

The curve described by Eq. (30) goes through the point (0,0) on the (φ,φ^*) plane as it is shown on Fig. 1. The figure also depicts curves of φ^* in dependence of φ for a number of semi-discrete compact schemes from [12, 17], their orders of approximation in space vary from four to eight. As it can be seen, the bicompact scheme possesses a better spectral resolution not only among schemes of the fourth order of approximation, but also among schemes of higher orders of approximation. It is also clear from Fig. 1 that the normalized group velocity $c_g/c=d\varphi^*/d\varphi$ [18] of wave packet energy propagation is greater or equal than one in case of the bicompact scheme. In case of the scheme CCS-T4 [12] the normalized group velocity is a non-negative quantity and it does not exceed unity. Compact schemes from [17] have a negative group velocity in the short-wave area.

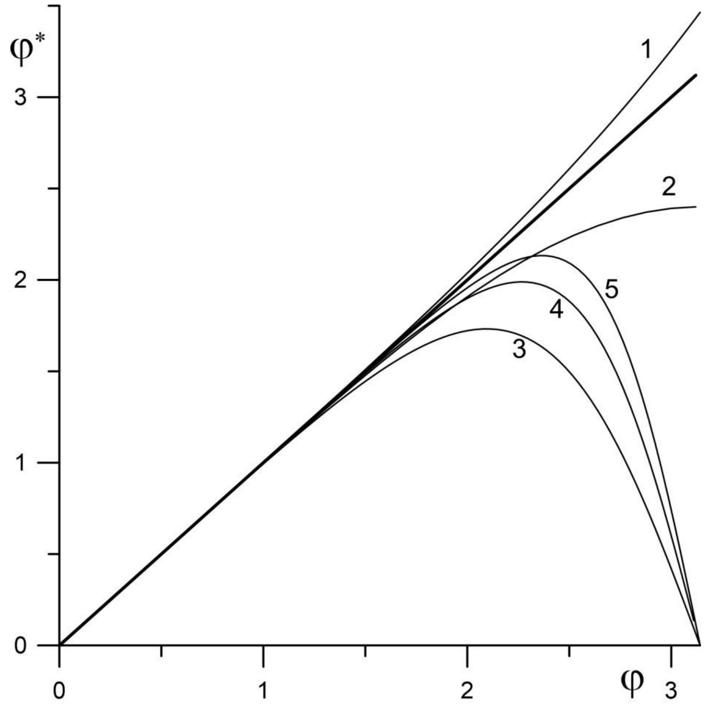

Fig. 1. Dimensionless effective wavenumber plotted against dimensionless exact wavenumber for various symmetric semi-discrete schemes. Curves: 1 – bicompact scheme of the fourth order of approximation; 2 – fourth order compact scheme CCS-T4 [12]; 3, 4, and 5 – tridiagonal classical fourth, sixth, and eighth order compact schemes respectively [17]. Thick straight line represents the ideal dependency $\varphi^* = \varphi$.

From Eqs. (28) and (30) we obtain the expression for the normalized numerical phase velocity of the semi-discrete bicompact scheme:

$$\frac{c^*}{c} = \frac{\varphi^*}{\varphi} = \frac{4\tan\left(\dfrac{\varphi}{2}\right)}{\varphi\left(1+\sqrt{1+\dfrac{4}{3}\tan^2\left(\dfrac{\varphi}{2}\right)}\right)}. \tag{31}$$

4. Fully discrete bicompact schemes

Finally any computation on a computer is done using a fully discrete scheme. Fourier analysis of semi-discrete schemes provides us with estimations of fully discrete schemes properties only at the limit of vanishing Courant numbers. The importance of fully discrete schemes study, i.e. study of interaction between approximations in space and time and their mutual influence on scheme properties, was discussed, for example, in [19, 20].

Two fully discrete bicompact schemes for the linear advection equation (10) are presented below, both in two-layer and three-layer forms.

Consider a fully discrete BiC4-BE scheme which is obtained from the semi-discrete scheme (11) by applying the implicit Euler method for time integration:

$$\begin{aligned} &(u_{j+1}^{n+1}+4U_{j+1/2}^{n+1}+u_j^{n+1})-(u_{j+1}^{n}+4U_{j+1/2}^{n}+u_j^{n})+6\kappa\left(u_{j+1}^{n+1}-u_j^{n+1}\right)=0,\\ &(u_{j+1}^{n+1}-u_j^{n+1})-(u_{j+1}^{n}-u_j^{n})+4\kappa\left(u_{j+1}^{n+1}-2U_{j+1/2}^{n+1}+u_j^{n+1}\right)=0, \end{aligned} \tag{32}$$

where n is time level number, $\kappa = c\tau/h$ is Courant number, τ is time step.

The scheme (32) consisting of two difference equations is a two-layer scheme for two mesh functions $\{u_j^n\}$, $\{U_{j+1/2}^n\}$. One may eliminate the function $\{U_{j+1/2}^n\}$ from this scheme and get the following three-layer bicompact scheme for the function $\{u_j^n\}$:

$$(12\kappa^2+6\kappa+1)u_{j+1}^{n+1}-(12\kappa^2-6\kappa+1)u_j^{n+1}-2(3\kappa+1)u_{j+1}^{n}-2(3\kappa-1)u_j^{n}+u_{j+1}^{n-1}-u_j^{n-1}=0. \tag{33}$$

Now let us consider a fully discrete BiC4-CN scheme [11] which is obtained from the semi-discrete scheme (11) by applying the trapezoid rule for time integration (the Crank-Nicolson method for time discretization) [7]:

$$\begin{aligned} &(u_{j+1}^{n+1}+4U_{j+1/2}^{n+1}+u_j^{n+1})-(u_{j+1}^{n}+4U_{j+1/2}^{n}+u_j^{n})+3\kappa\left[(u_{j+1}^{n+1}-u_j^{n+1})+(u_{j+1}^{n}-u_j^{n})\right]=0,\\ &(u_{j+1}^{n+1}-u_j^{n+1})-(u_{j+1}^{n}-u_j^{n})+2\kappa\left[(u_{j+1}^{n+1}-2U_{j+1/2}^{n+1}+u_j^{n+1})+(u_{j+1}^{n}-2U_{j+1/2}^{n}+u_j^{n})\right]=0. \end{aligned} \tag{34}$$

By eliminating the mesh function $\{U_{j+1/2}^n\}$ from the two-layer scheme (34) one may transform it into the three-layer bicompact scheme for the mesh function $\{u_j^n\}$:

$$\begin{aligned} &(3\kappa^2+3\kappa+1)u_{j+1}^{n+1}-(3\kappa^2-3\kappa+1)u_j^{n+1}+2(3\kappa^2-1)u_{j+1}^{n}-2(3\kappa^2-1)u_j^{n}+\\ &\quad+(3\kappa^2-3\kappa+1)u_{j+1}^{n-1}-(3\kappa^2+3\kappa+1)u_j^{n-1}=0. \end{aligned} \tag{35}$$

It is important to note that difference orders of bicompact schemes (32) and (34) in two-layer form are equal to unity in both time and space, i.e. they coincide with orders in t and x of the linear advection equation (10). By difference order of a scheme in space we mean the difference between the number of stencil nodes in the x direction and the number of equations in the scheme. The number of time levels in the scheme minus one is called difference order of a scheme in time. The equality between difference and differential orders results in the same number of initial and boundary conditions required for numerical and differential problems. For instance, if an initial/boundary value problem for the scheme (32) is stated in the first quadrant of the (x, t) plane, then one should state one initial condition at $t = 0$ and one boundary condition at $x = 0$.

The opportunity to transform a two-layer bicompact scheme on the spatial stencil of two integer and one half-integer nodes into a three-layer scheme on the stencil of two integer nodes is determined by the first difference order of the three-layer bicompact scheme with respect to x. However, the three-layer scheme of the second difference order in t requires two initial conditions: one of them should be stated at the zero time level at $t = 0$ and the other one should be stated at the first time level. For an initial condition at the first time level we propose to use the solution provided by the corresponding two-layer bicompact scheme.

5. Fourier analysis of fully discrete bicompact schemes

The Fourier analysis [21] may be done for two-layer bicompact schemes (32) and (34) straightforward. However, it is much easier to carry out this analysis for three-layer schemes (33) and (35). Such an analysis is developed below.

Following the practical guidelines of L.N. Trefethen [22] we carry out a Fourier analysis of bicompact schemes using not some tedious derivations based on Fourier transform, but a more handy method based on substituting test mesh functions

$$\begin{aligned} &u_j^n = \lambda^n \exp(ij\varphi), \lambda = \rho \exp\left(-ikc^*\tau\right) = \rho \exp\left(-i\varphi\kappa c^*/c\right), \\ &\rho = |\lambda|, \varphi = kh, \kappa = c\tau/h, \end{aligned} \qquad (36)$$

into numerical schemes for the advection equation (10). Here λ is the so-called amplification factor [20-22] which is a complex number in general case, ρ is the absolute value of this factor. Note that the numerical problem for the Eq. (10) is considered along the whole x-axis.

Results for the Fourier analysis of the three-layer bicompact schemes BiC4-BE (33) and BiC4-CN (35) are described further. Both schemes are absolute stable: the advection equation is integrated with respect to spatial variable by the A-stable Lobatto IIIA scheme [7], while the integration with respect to time is done by the L-stable implicit Euler method and the A-stable trapezoid rule [7].

The BiC4-BE scheme. Substituting the test function (36) into the scheme (33) yields the characteristic equation for the amplification factor λ:

$$(12\kappa^2+1)\lambda - i6\kappa\cot\left(\frac{\varphi}{2}\right)(\lambda-1) - 2 + \frac{1}{\lambda} = 0\,. \qquad (37)$$

By making the following substitution

$$\lambda = \frac{1-i\xi}{1+\xi^2} \qquad (38)$$

into Eq. (37) we obtain a quadratic equation for the quantity ξ:

$$\xi^2 + 6\kappa\cot(\varphi/2)\xi - 12\kappa^2 = 0\,. \qquad (39)$$

The discriminant of this equation is greater than zero, thus it has two real roots

$$\xi_1 = 3\kappa\left(\sqrt{\cot^2\left(\frac{\varphi}{2}\right)+\frac{4}{3}}-\cot\left(\frac{\varphi}{2}\right)\right), \quad \xi_2 = -3\kappa\left(\sqrt{\cot^2\left(\frac{\varphi}{2}\right)+\frac{4}{3}}+\cot\left(\frac{\varphi}{2}\right)\right).$$

Let us change $\cot(\varphi/2)$ for $\tan(\varphi/2)$ in formulas for these roots:

$$\xi_1 = \frac{4\kappa\tan\left(\frac{\varphi}{2}\right)}{1+\sqrt{1+\frac{4}{3}\tan^2\left(\frac{\varphi}{2}\right)}}, \quad \xi_2 = -\frac{4\kappa\tan\left(\frac{\varphi}{2}\right)}{\sqrt{1+\frac{4}{3}\tan^2\left(\frac{\varphi}{2}\right)}-1}. \tag{40}$$

The first root in Eq. (40) is physically correct: its normalized numerical phase velocity

$$\frac{c^*}{c} = -\frac{1}{\varphi\kappa}\arg\lambda = \frac{1}{\varphi\kappa}\arctan\xi \tag{41}$$

tends to one if $\varphi \to 0$, i.e. if $h \to 0$ for a fixed value of the wavenumber *k*. The second root in Eq. (40) is a "parasite" one, its influence on the numerical solution can be eliminated by a correct choice of initial and boundary conditions for the numerical problem (see [11, 13, 14]). By substitution of the first root into Eqs. (38) and (41) we obtain

$$\rho = |\lambda| = \frac{1}{\sqrt{1+\xi_1^2}}, \quad \frac{c^*}{c} = \frac{1}{\varphi\kappa}\arctan\xi_1 = \frac{1}{\varphi\kappa}\arctan\left(\frac{4\kappa\tan\left(\frac{\varphi}{2}\right)}{1+\sqrt{1+\frac{4}{3}\tan^2\left(\frac{\varphi}{2}\right)}}\right). \tag{42}$$

From Eqs. (40), (42) it follows that

$$\rho = 1, \quad \frac{c^*}{c} = \frac{4\tan(\varphi/2)}{\varphi\left(1+\sqrt{1+\frac{4}{3}\tan^2\left(\frac{\varphi}{2}\right)}\right)},$$

if the Courant number κ goes to zero. The last formula exactly matches the Eq. (31) for the numerical phase velocity of the semi-discrete bicompact scheme.

Taking into account Eq. (42) leads us to the normalized group velocity

$$\frac{c_g}{c}=\frac{d}{d\varphi}\left(\varphi\frac{c^*}{c}\right)=\frac{2\left(1+1\Big/\sqrt{1+\frac{4}{3}\tan^2\left(\frac{\varphi}{2}\right)}\right)}{16\kappa^2\sin^2\left(\frac{\varphi}{2}\right)+\left(\cos\left(\frac{\varphi}{2}\right)+\sqrt{\cos^2\left(\frac{\varphi}{2}\right)+\frac{4}{3}\sin^2\left(\frac{\varphi}{2}\right)}\right)^2}. \qquad (43)$$

From Eq. (43) we see that the group velocity is a positive value for all Courant numbers belonging to the interval $\varphi\in[0,\pi]$.

Figs. 2 and 3 represent plots of the amplification factor absolute value, numerical phase and group velocities as functions of the dimensionless wavenumber for the BiC4-BE scheme at different Courant numbers.

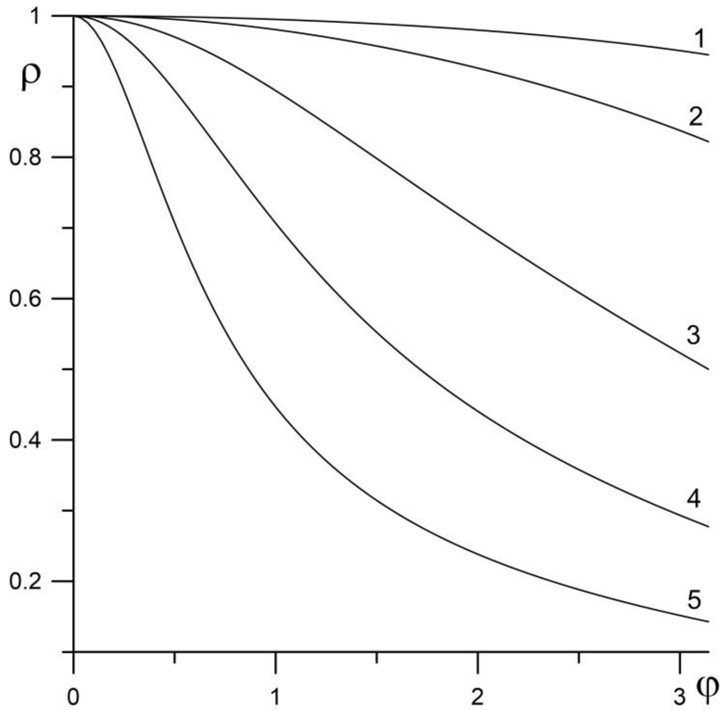

Fig. 2. The amplification factor absolute value plotted against the dimensionless wavenumber φ at different Courant numbers. Curves 1-5 correspond to the Courant number κ equal to 0.1, 0.2, 0.5, 1.0, and 2.0 respectively.

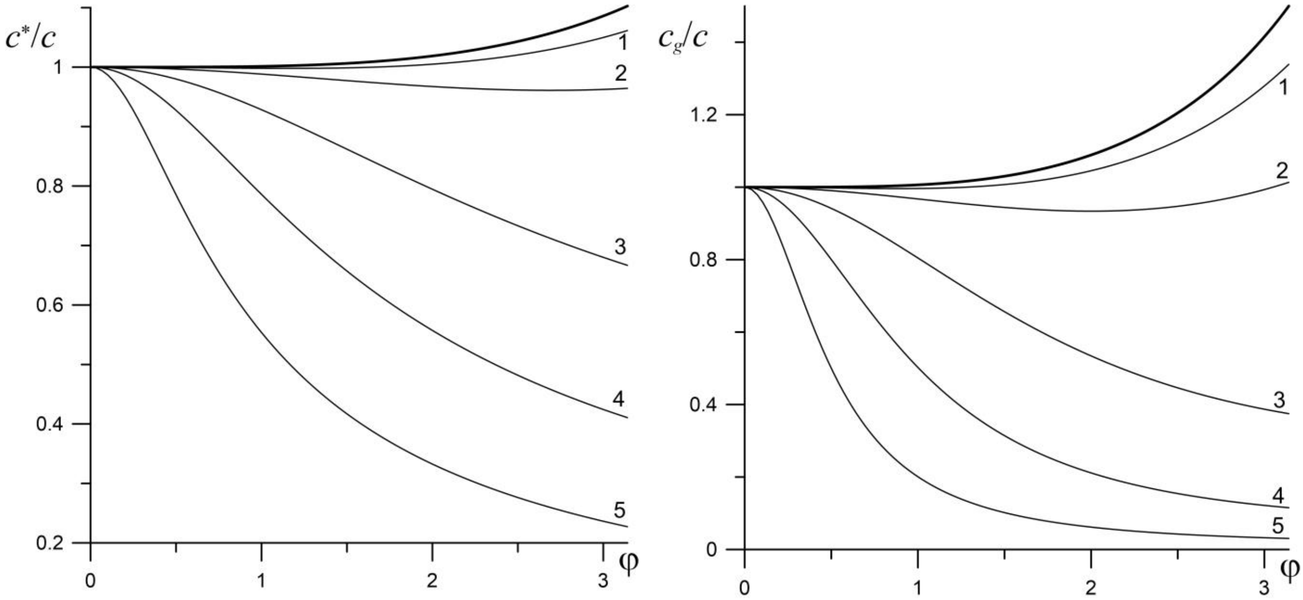

Fig. 3. Numerical phase and group velocities plotted against the dimensionless wavenumber φ at different Courant numbers. Curves 1-5 correspond to the Courant number κ equal to 0.1, 0.2, 0.5, 1.0, and 2.0 respectively. Thick curves represent dependencies for the semi-discrete bicompact scheme.

The BiC4-CN scheme. Substitution of the test function (36) into the scheme (35) leads to the characteristic equation for the amplification factor λ:

$$(3\kappa^2+1)\left(\lambda+\frac{1}{\lambda}\right)-i3\kappa\cot\left(\frac{\varphi}{2}\right)\left(\lambda-\frac{1}{\lambda}\right)+2(3\kappa^2-1)=0\,. \tag{44}$$

Suggest the amplification factor to be

$$\lambda=e^{i\theta}\,. \tag{45}$$

Then Eq. (44) yields the equation for the quantity θ:

$$(3\kappa^2+1)\cos\theta+3\kappa\cot(\varphi/2)\sin\theta+3\kappa^2-1=0\,. \tag{46}$$

One may transform this equation into a quadratic equation for $\cot(\theta/2)$:

$$3\kappa^2\cot^2\left(\frac{\theta}{2}\right)+3\kappa\cot\left(\frac{\varphi}{2}\right)\cot\left(\frac{\theta}{2}\right)-1=0\,. \tag{47}$$

The discriminant of this quadratic equation is greater than zero, thus it has two real roots

$$\cot\left(\frac{\theta_1}{2}\right)=-\frac{1}{2\kappa}\left(\cot\left(\frac{\varphi}{2}\right)+\sqrt{\cot^2\left(\frac{\varphi}{2}\right)+\frac{4}{3}}\right),\ \cot\left(\frac{\theta_2}{2}\right)=\frac{1}{2\kappa}\left(\sqrt{\cot^2\left(\frac{\varphi}{2}\right)+\frac{4}{3}}-\cot\left(\frac{\varphi}{2}\right)\right). \tag{48}$$

By changing cotangents by tangents in Eq. (48) we obtain

$$\tan\left(\frac{\theta_1}{2}\right) = -\frac{2\kappa\tan\left(\frac{\varphi}{2}\right)}{1+\sqrt{1+\frac{4}{3}\tan^2\left(\frac{\varphi}{2}\right)}}, \quad \tan\left(\frac{\theta_2}{2}\right) = \frac{2\kappa\tan\left(\frac{\varphi}{2}\right)}{\sqrt{1+\frac{4}{3}\tan^2\left(\frac{\varphi}{2}\right)}-1}. \qquad (49)$$

Because quantities θ_1 and θ_2 are real, the absolute value ρ of the amplification factor λ equals to one according to Eq. (45). This means that the BiC4-CN scheme is non-dissipative.

The first root in Eq. (49) is physically correct: its normalized numerical phase velocity

$$\frac{c^*}{c} = -\frac{1}{\varphi\kappa}\arg\lambda = -\frac{\theta}{\varphi\kappa}, \qquad (50)$$

goes to one as $\varphi \to 0$, i.e. as $h \to 0$ for a fixed value of the wavenumber *k*. The other root is a "parasite" one, its influence on the numerical solution can be eliminated by a correct choice of initial and boundary conditions for the numerical problem (see [11, 13, 14]). By substituting the first root θ_1 into Eq. (50) we obtain

$$\frac{c^*}{c} = -\frac{\theta_1}{\varphi\kappa} = \frac{2}{\varphi\kappa}\arctan\left(\frac{2\kappa\tan\left(\frac{\varphi}{2}\right)}{1+\sqrt{1+\frac{4}{3}\tan^2\left(\frac{\varphi}{2}\right)}}\right). \qquad (51)$$

From Eq. (51) it follows that

$$\frac{c^*}{c} = \frac{4\tan\left(\frac{\varphi}{2}\right)}{\varphi\left(1+\sqrt{1+\frac{4}{3}\tan^2\left(\frac{\varphi}{2}\right)}\right)},$$

as the Courant number κ tends to zero. The last formula exactly matches the Eq. (31) for the numerical phase velocity of the semi-discrete bicompact scheme.

Using Eq. (51) we obtain the normalized group velocity

$$\frac{c_g}{c}=\frac{d}{d\varphi}\left(\varphi\frac{c^*}{c}\right)=\frac{2\left(1+1\Big/\sqrt{1+\frac{4}{3}\tan^2\left(\frac{\varphi}{2}\right)}\right)}{4\kappa^2\sin^2\left(\frac{\varphi}{2}\right)+\left(\cos\left(\frac{\varphi}{2}\right)+\sqrt{\cos^2\left(\frac{\varphi}{2}\right)+\frac{4}{3}\sin^2\left(\frac{\varphi}{2}\right)}\right)^2}. \qquad (52)$$

From Eq. (52) we see that the group velocity is a positive value for all Courant numbers belonging to the interval $\varphi\in[0,\pi]$.

A comparison between formulae (42), (43) and formulae (51), (52) suggests that the plots of numerical phase and group velocities as the functions of the dimensionless wavenumber for the BiC4-CN scheme with the fixed Courant number $\kappa=\kappa_0$ are the same as those for the BiC4–BE scheme taken at the Courant number $\kappa=\kappa_0/2$.

Fig. 4 represents plots of numerical phase and group velocities as functions of the dimensionless wavenumber for the BiC4-CN scheme at different Courant numbers.

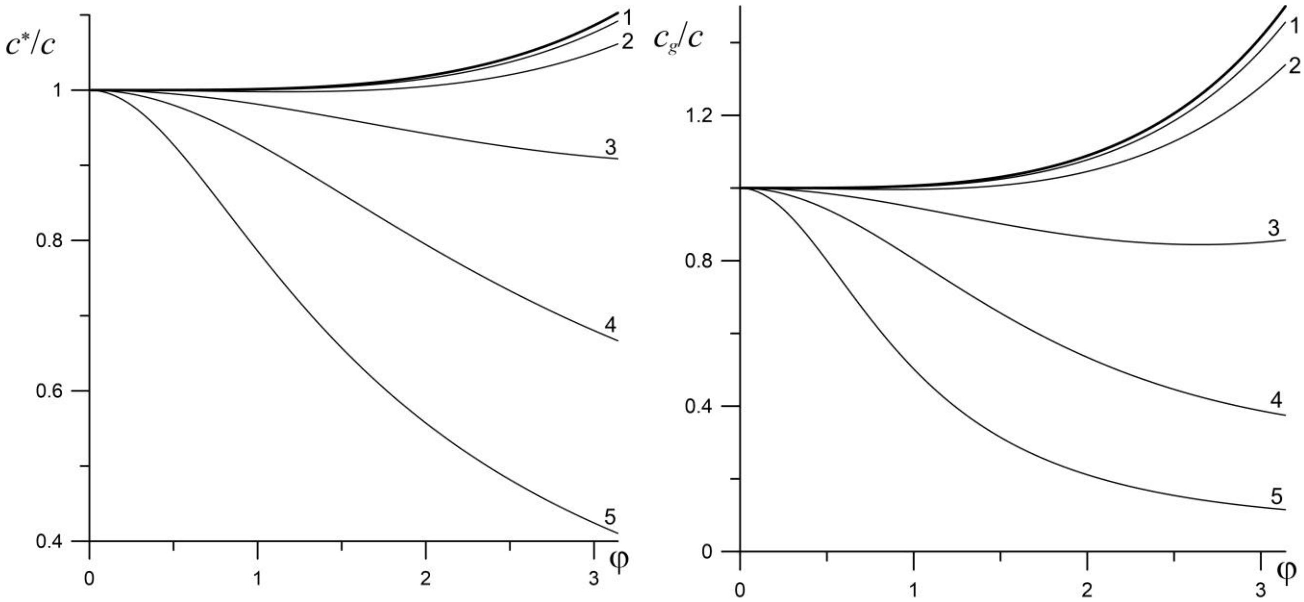

Fig. 4. Numerical phase and group velocities plotted against the dimensionless wavenumber φ at different Courant numbers. Curves 1-5 correspond to the Courant number κ equal to 0.1, 0.2, 0.5, 1.0, and 2.0 respectively. Thick curves represent dependencies for the semi-discrete bicompact scheme.

6. Comparison of bicompact schemes with some known numerical schemes for advection equation

In this section we compare dispersive and dissipative properties of bicompact schemes BiC4-BE and BiC4-CN to those properties of two-layer three-point compact schemes of the fourth order of approximation in space, the three-layer Leapfrog scheme [23], and the three-layer Iserles scheme [24]. The two-layer “CABARET” scheme [25, 26] is reduced to the latter scheme on a uniform space-time mesh

Three-point compact schemes. If we integrate Eq. (1) at $t = const$ along the interval $[x_{j-1}, x_{j+1}]$ and approximate the integral of u using the Simpson’s quadrature rule, we obtain the semi-discrete three-point compact scheme of the fourth order of approximation in space [17]:

$$\frac{h}{3}\frac{d}{dt}\left(u_{j-1} + 4u_j + u_{j+1}\right) + f_{j+1} - f_{j-1} = 0. \tag{53}$$

This scheme may be derived by other methods. For example, one may use the finite element Galerkin method, as it is done in the monograph [21]. In case of the linear advection equation (10) the scheme (53) takes the form of

$$\frac{h}{3}\frac{d}{dt}\left(u_{j-1} + 4u_j + u_{j+1}\right) + c\left(u_{j+1} - u_{j-1}\right) = 0. \tag{54}$$

Below we present a Fourier analysis of the two fully discrete compact schemes C4-BE and C4-CN for the linear advection equation (10). The C4-BE scheme is constructed by applying the implicit Euler method for time integration in the semi-discrete scheme (54), and the C4-CN scheme – by applying the trapezoid rule [7] to it.

(a) The C4-BE scheme. As it is mentioned in the paragraph above, the integration of Eq. (54) with respect to time by the implicit Euler method yields the fully discrete finite difference scheme C4-BE:

$$u_{j-1}^{n+1} + 4u_j^{n+1} + u_{j+1}^{n+1} - \left(u_{j-1}^{n} + 4u_j^{n} + u_{j+1}^{n}\right) + 3\kappa\left(u_{j+1}^{n+1} - u_{j-1}^{n+1}\right) = 0. \tag{55}$$

Substitution of the test function (36) into the scheme (55) gives us the linear characteristic equation for the amplification factor λ. Its solution holds

$$\lambda = \frac{1 - i\xi}{1 + \xi^2}, \quad \xi = \frac{3\kappa \sin\varphi}{2 + \cos\varphi}. \tag{56}$$

From the formula (56) we find ρ, c^*/c, and c_g/c:

$$\rho = |\lambda| = \frac{1}{\sqrt{1+\xi^2}}, \quad \frac{c^*}{c} = -\frac{1}{\varphi\kappa}\arg\lambda = \frac{1}{\varphi\kappa}\arctan\xi = \frac{1}{\varphi\kappa}\arctan\left(\frac{3\kappa\sin\varphi}{2+\cos\varphi}\right), \tag{57}$$

$$\frac{c_g}{c} = \frac{d}{d\varphi}\left(\varphi\frac{c^*}{c}\right) = \frac{3(1+2\cos\varphi)}{9\kappa^2\sin^2\varphi + (2+\cos\varphi)^2}. \tag{58}$$

Plots of the amplification factor absolute value, phase and group velocities as functions of the dimensionless wavenumber for the C4-BE scheme at different Courant numbers are shown on Figs. 5 and 6. These figures also represent the curves for the BiC4-BE scheme. The data given on Fig. 5 clearly shows that the dissipative C4-BE scheme damps the high wavenumber harmonics around $\varphi \approx \pi$ rather poorly. On contrary, the harmonics with the highest wavenumbers $\varphi \approx \pi$ resolvable on the mesh are those most strongly damped by the BiC4-BE scheme. This effect coincides with the monotonicity property of the BiC4-BE scheme studied in [6, 8]. It follows from the plots on Fig. 6 that the BiC4-BE scheme eliminates a substantial shortcoming of the C4-BE scheme connected with negative values of group velocity at $\varphi > 3\pi/4$. Schemes with such undesired property are very sensitive to mesh smoothness. Theses schemes require spatial meshes that are less than 8-10% non-uniform (see [4]; percentage denotes value of relation between lengths of neighboring cells). As the allowed rate of mesh refining/coarsening is exceeded, strong reflected parasite waves are generated by such schemes.

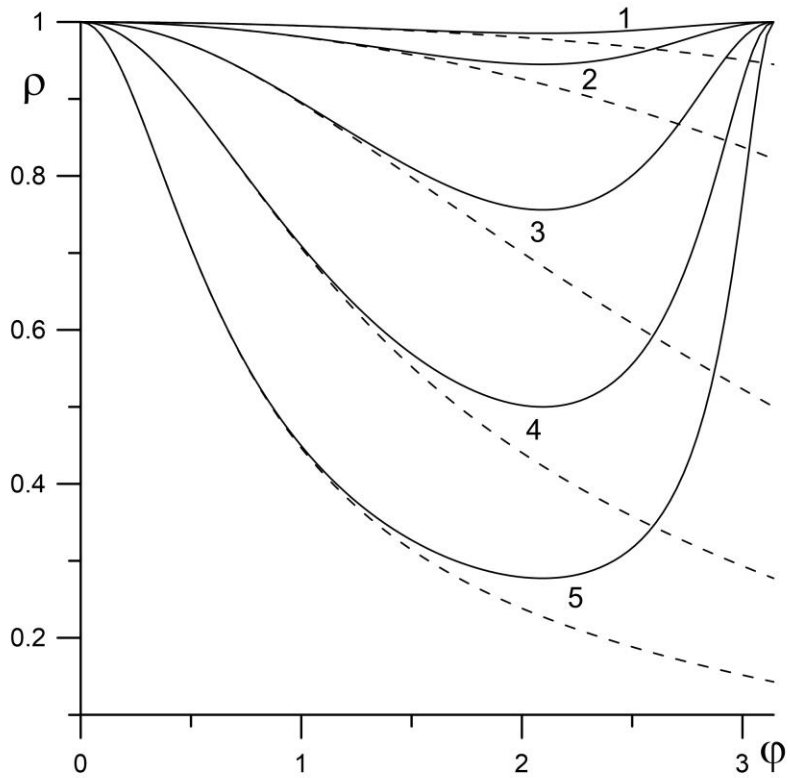

Fig. 5. The amplification factor absolute value plotted against the dimensionless wavenumber φ at different Courant numbers. Curves 1-5 correspond to the Courant number κ equal to 0.1, 0.2, 0.5, 1.0, and 2.0 respectively. Solid curves correspond to the C4-BE scheme, while dashed ones correspond to the BiC4-BE scheme.

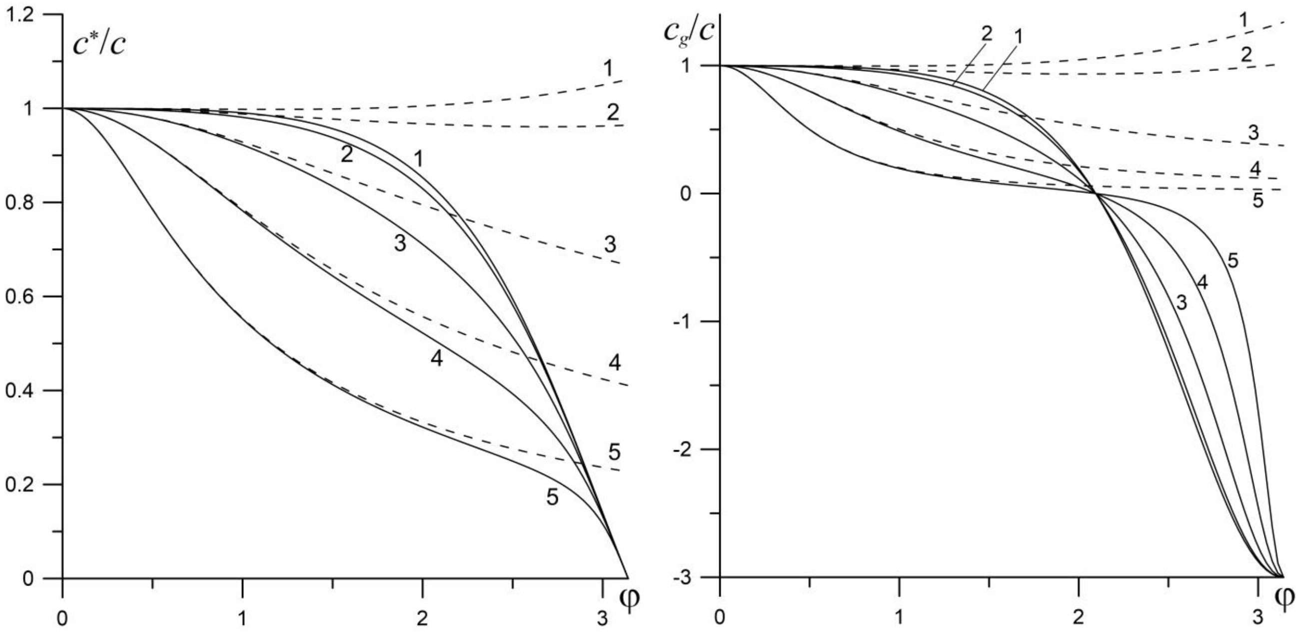

Fig. 6. Numerical phase and group velocities plotted against the dimensionless wavenumber φ at different Courant numbers. Curves 1-5 correspond to the Courant number κ equal to 0.1, 0.2, 0.5, 1.0, and 2.0 respectively. Solid curves correspond to the C4-BE scheme, while dashed ones correspond to the BiC4-BE scheme.

(b) The C4-CN scheme. Integration of Eq. (54) by the trapezoid rule yields the fully discrete numerical scheme C4-CN:

$$u_{j-1}^{n+1}+4u_j^{n+1}+u_{j+1}^{n+1}-\left(u_{j-1}^{n}+4u_j^{n}+u_{j+1}^{n}\right)+\frac{3}{2}\kappa\left(u_{j+1}^{n+1}-u_{j-1}^{n+1}+u_{j+1}^{n}-u_{j-1}^{n}\right)=0. \tag{59}$$

Once again, we obtain the characteristic equation for the amplification factor λ by substituting the test function (36) into the scheme (59):

$$\frac{1-\lambda}{1+\lambda}=i\,\frac{3\kappa\sin\varphi}{2(2+\cos\varphi)}. \tag{60}$$

Given the amplification factor has the following form:

$$\lambda=e^{i\theta}, \tag{61}$$

we easily obtain the solution for the quantity θ from Eq. (60):

$$\theta=-2\arctan\left(\frac{3\kappa\sin\varphi}{2(2+\cos\varphi)}\right). \tag{62}$$

Formulae (61), (62) result into the equality $\rho=|\lambda|=1$, thus the C4-CN scheme is stable and non-dissipative. From these formulae we also obtain expressions for numerical phase and group velocities:

$$\frac{c^*}{c} = -\frac{1}{\varphi\kappa}\arg\lambda = -\frac{\theta}{\varphi\kappa} = \frac{2}{\varphi\kappa}\arctan\left(\frac{3\kappa\sin\varphi}{2(2+\cos\varphi)}\right), \tag{63}$$

$$\frac{c_g}{c} = \frac{d}{d\varphi}\left(\varphi\frac{c^*}{c}\right) = \frac{3(1+2\cos\varphi)}{\frac{9}{4}\kappa^2\sin^2\varphi + (2+\cos\varphi)^2}. \tag{64}$$

A comparison between formulae (63), (64) and formulae (57), (58) suggests that the plots of numerical phase and group velocities as the functions of the dimensionless wavenumber for the C4-CN scheme with the fixed Courant number $\kappa = \kappa_0$ are the same as those for the C4-BE scheme taken at the Courant number $\kappa = \kappa_0/2$.

Fig. 7 depicts plots of numerical phase and group velocities as functions of the dimensionless wavenumber for the C4-CN scheme at different Courant numbers. This figure also shows the plots for the BiC4-CN scheme. It is clear from the Fig. 7 that the BiC4-CN scheme fixes the substantial shortcoming of the C4-CN scheme connected with negative values of group velocity at $\varphi > 3\pi/4$.

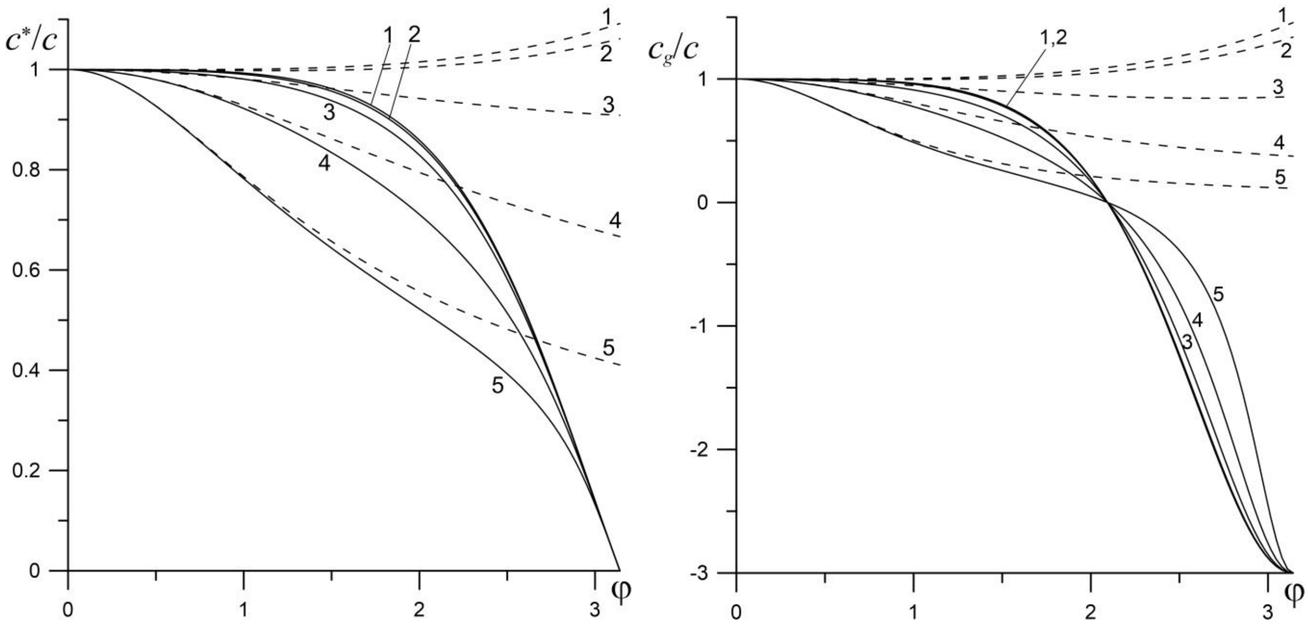

Fig. 7. Numerical phase and group velocities plotted against the dimensionless wavenumber φ at different Courant numbers. Curves 1-5 correspond to the Courant number κ equal to 0.1, 0.2, 0.5, 1.0, and 2.0 respectively. Solid curves correspond to the C4-CN scheme, while dashed ones correspond to the BiC4-CN scheme.

The Leapfrog scheme. This three-layer scheme has the symmetrical cross-like space-time stencil on the (x, t) plane. In case of the linear advection equation (10) the Leapfrog scheme takes the following form:

$$u_j^{n+1} - u_j^{n-1} + \kappa\left(u_{j+1}^n - u_{j-1}^n\right) = 0. \tag{65}$$

In linear approximation the Leapfrog scheme is stable at Courant numbers less than one.

Substitution of the test function (36) into the scheme (65) leads to the characteristic equation for the amplification factor λ:

$$\lambda^2 + i(2\kappa\sin\varphi)\lambda - 1 = 0\,. \tag{66}$$

Quadratic Eq. (66) has two complex roots:

$$\lambda_1 = \sqrt{1-\kappa^2\sin^2\varphi} - i\kappa\sin\varphi, \quad \lambda_2 = -\sqrt{1-\kappa^2\sin^2\varphi} - i\kappa\sin\varphi\,. \tag{67}$$

Absolute values of these roots are equal to one, therefore the Leapfrog scheme is non-dissipative. The first root from Eq. (67) is physically correct: its normalized numerical phase velocity

$$\frac{c^*}{c} = -\frac{1}{\varphi\kappa}\arg\lambda \tag{68}$$

goes to one as $\varphi \to 0$, i.e. as $h \to 0$ for a fixed value of the wavenumber *k*. The other root is a “parasite” one, its influence on the numerical solution can be eliminated by a correct choice of initial and boundary conditions for the numerical problem.

By substituting the root λ_1 into the formula (68) we find the normalized numerical phase velocity

$$\frac{c^*}{c} = -\frac{1}{\varphi\kappa}\arg\lambda_1 = \frac{1}{\varphi\kappa}\arctan\left(\frac{\kappa\sin\varphi}{\sqrt{1-\kappa^2\sin^2\varphi}}\right), \tag{69}$$

and then the normalized group velocity

$$\frac{c_g}{c} = \frac{d}{d\varphi}\left(\varphi\frac{c^*}{c}\right) = \frac{\cos\varphi}{\sqrt{1-\kappa^2\sin^2\varphi}}\,. \tag{70}$$

Fig. 8 shows plots of numerical phase and group velocities as functions of the dimensionless wavenumber for the Leapfrog scheme at different Courant numbers. This figure also represents the plots for the BiC4-CN scheme. Fig. 8 makes it clear that the Leapfrog scheme has the substantial shortcoming connected with negative values of group velocity at $\varphi > \pi/2$.

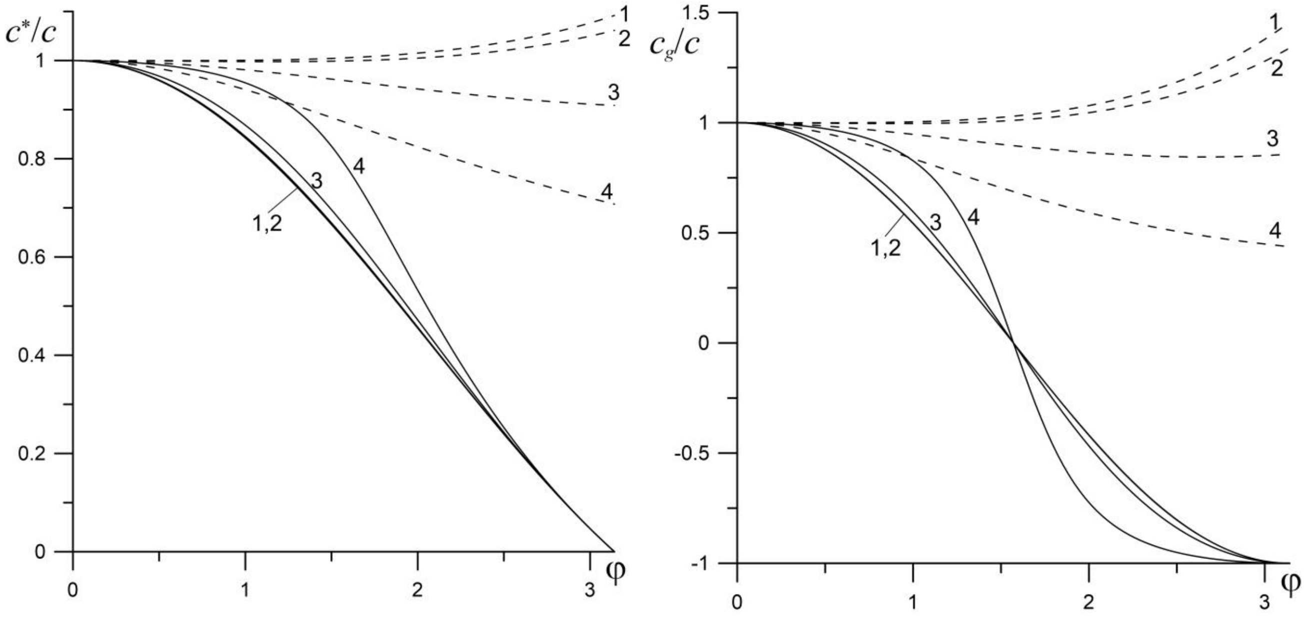

Fig. 8. Numerical phase and group velocities plotted against the dimensionless wavenumber φ at different Courant numbers. Curves 1-4 correspond to the Courant number κ equal to 0.1, 0.2, 0.5, and 0.9 respectively. Solid curves correspond to the Leapfrog scheme, while dashed ones correspond to the BiC4-CN scheme.

The Iserles scheme (the "CABARET" scheme). This three-layer finite difference scheme was first proposed in [24]. In case of the linear advection equation (10) it is written as

$$\frac{1}{2}\left(u_{j+1}^{n+1}-u_{j+1}^{n}+u_{j}^{n}-u_{j}^{n-1}\right)+\kappa\left(u_{j+1}^{n}-u_{j}^{n}\right)=0\,. \tag{71}$$

The space-time stencil of the Iserles scheme is not symmetrical. The scheme can be classified as an upwind one, i.e. a scheme which depends from advection direction (sign of the phase velocity c). The Iserles scheme is stable if Courant number is less or equal than one.

Substitution of the test function (36) into the scheme (71) yields the characteristic equation for the amplification factor λ:

$$\lambda^2-(1-2\kappa)\left(1-e^{-i\varphi}\right)\lambda-e^{-i\varphi}=0\,. \tag{72}$$

The characteristic equation (72) for the scheme (71) is the same as for the two-layer "CABARET" scheme [26].

By applying the Vieta's formulae to Eq. (72) we obtain two equations for its two roots λ_1 and λ_2:

$$\lambda_1+\lambda_2=(1-2\kappa)(1-e^{-i\varphi}), \tag{73}$$

$$\lambda_1\lambda_2 = -e^{-i\varphi} \tag{74}$$

Let us find the solution of Eqs. (73), (74) in the form

$$\lambda_1 = e^{-i\varphi_1},\ \lambda_2 = -e^{-i\varphi_2}\,. \tag{75}$$

Then we substitute Eq. (75) into Eq. (73), set equal real and imaginary parts of left- and right-hand sides of Eq. (73), and after some simple calculations obtain the system of two equations defining φ_1 and φ_2:

$$\sin\left(\frac{\varphi_1+\varphi_2}{2}\right)\sin\left(\frac{\varphi_2-\varphi_1}{2}\right) = (1-2\kappa)\sin^2\left(\frac{\varphi}{2}\right), \tag{76}$$

$$\sin\left(\frac{\varphi_2-\varphi_1}{2}\right)\cos\left(\frac{\varphi_1+\varphi_2}{2}\right) = (1-2\kappa)\sin\left(\frac{\varphi}{2}\right)\cos\left(\frac{\varphi}{2}\right). \tag{77}$$

As we substitute Eq. (75) into Eq. (74), we obtain the third equation for φ_1 and φ_2:

$$\varphi_1 + \varphi_2 = \varphi\,. \tag{78}$$

Interestingly, the system of three equations (76)-(78) for φ_1 and φ_2 turns out to be consistent. If we use Eq. (78) to simplify the left-hand side of Eq. (76) and drop out the common factor $\sin(\varphi/2)$ from the both sides of the equation, we finally arrive at the equation

$$\sin\left(\frac{\varphi_2-\varphi_1}{2}\right) = (1-2\kappa)\sin\left(\frac{\varphi}{2}\right). \tag{79}$$

Alternatively, if we substitute Eq. (78) into the left-hand side of Eq. (77) and drop out the common factor $\cos(\varphi/2)$ from left- and right-hand sides of the equation, we obtain Eq. (79) again. Thus, there are two independent Eqs. (78) and (79) for two sought quantities φ_1 and φ_2. The solution of these equations holds

$$\varphi_1 = \frac{\varphi}{2} - \arcsin\left((1-2\kappa)\sin\left(\frac{\varphi}{2}\right)\right),\ \varphi_2 = \frac{\varphi}{2} + \arcsin\left((1-2\kappa)\sin\left(\frac{\varphi}{2}\right)\right). \tag{80}$$

From Eqs. (75) and (80) we obtain analytical expressions for roots of characteristic Eq. (72):

$$\lambda_1 = \exp\left\{-i\left[\frac{\varphi}{2} - \arcsin\left((1-2\kappa)\sin\left(\frac{\varphi}{2}\right)\right)\right]\right\}, \tag{81}$$

$$\lambda_2 = -\exp\left\{-i\left[\frac{\varphi}{2} + \arcsin\left((1-2\kappa)\sin\left(\frac{\varphi}{2}\right)\right)\right]\right\}. \tag{82}$$

These roots have the absolute value of one, therefore the Iserles scheme is non-dissipative. The first root from Eqs. (81), (82) is physically correct: its normalized numerical phase velocity

$$\frac{c^*}{c} = -\frac{1}{\varphi\kappa}\arg\lambda \tag{83}$$

tends to one as $\varphi \to 0$, i.e. as $h \to 0$ for a fixed value of the wavenumber *k*. The other root is a "parasite" one, its influence on the numerical solution can be eliminated by setting up consistent initial conditions at zero and first time levels in the three-level scheme [25, 26]. We find the normalized numerical phase velocity by substituting λ_1 into Eq. (83):

$$\frac{c^*}{c} = -\frac{1}{\varphi\kappa}\arg\lambda_1 = \frac{\varphi_1}{\varphi\kappa} = \frac{1}{\kappa}\left[\frac{1}{2} - \frac{1}{\varphi}\arcsin\left((1-2\kappa)\sin\left(\frac{\varphi}{2}\right)\right)\right], \tag{84}$$

and after that we find the normalized numerical group velocity:

$$\frac{c_g}{c} = \frac{d}{d\varphi}\left(\varphi\frac{c^*}{c}\right) = \frac{1}{2\kappa}\left(1 - \frac{(1-2\kappa)\cos\left(\frac{\varphi}{2}\right)}{\sqrt{1-(1-2\kappa)^2\sin^2\left(\frac{\varphi}{2}\right)}}\right). \tag{85}$$

At the limit of zero Courant number we obtain the following formulae for c^*/c and c_g/c from Eqs. (84), (85):

$$\frac{c^*}{c} = \frac{2}{\varphi}\tan\left(\frac{\varphi}{2}\right), \quad \frac{c_g}{c} = \frac{1}{\cos^2(\varphi/2)} \tag{86}$$

As it follows from these formulae, the Iserles scheme has a singularity at the Courant number $\kappa = 0$: phase and group velocities of the scheme go to infinity as $\varphi \to \pi$.

Figs. 9 and 10 represent plots of numerical phase and group velocities as functions of the dimensionless wavenumber for the Iserles scheme at different Courant numbers. The figures also show the plots for the BiC4-CN scheme.

A comparison between graphs from these figures leads to the conclusion that the BiC4-CN scheme has a better spectral resolution than the Iserles scheme for Courant numbers $0 \le \kappa \le 0.4$, while for $0.5 \le \kappa \le 1.0$ a better spectral resolution is possessed by the Iserles scheme. This is not surprising since, on the one hand, the Iserles scheme has the mentioned above singularity at the Courant number $\kappa = 0$ while, on the other hand, this scheme provides the exact solution of the advection equation (10) for Courant numbers equal to 0.5 and 1 [25, 26].

Note that, considering linear hyperbolic equations with variable coefficients and quasilinear hyperbolic equations, the condition $0 \le \kappa \le 0.4$ for the local Courant number κ is easier to be maintained on the mesh than the condition $0.5 \le \kappa \le 1.0$.

7. Conclusion

In this work, the Fourier analysis of the two fully discrete bicompact scheme of the fourth order of approximation in space for hyperbolic equations is presented. The analysis is carried out in case of the model linear advection equation. Prior to the Fourier analysis the two-level bicompact finite difference schemes each consisting of two difference equations for two mesh functions, one defined over integer nodes, the other over half-integer nodes, are transformed into the three-level schemes each consisting of one difference equation for one mesh function defined over integer nodes. The results of the Fourier analysis are supplied with figures of bicompact schemes' dispersion and dissipation characteristics plotted as functions of dimensionless wavenumber and Courant numbers. A comparison with dispersive and dissipative properties of other widely used numerical schemes for hyperbolic equations is done. It is shown that bicompact schemes possess one of the best spectral resolutions among the compared numerical schemes.

In addition, it is explained in what sense bicompact schemes are nonstandard, they are compared with other known compact schemes.

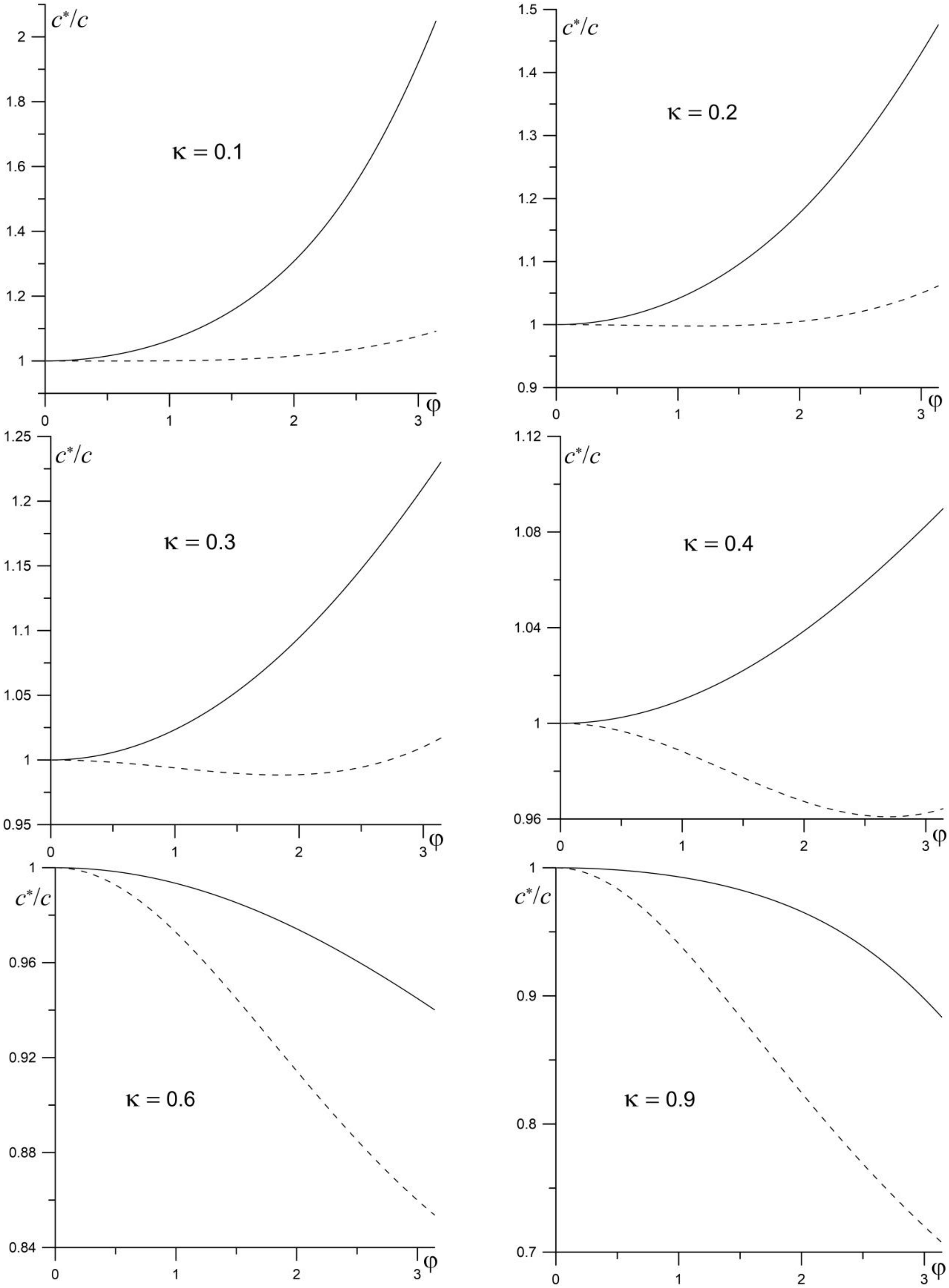

Fig. 9. Numerical phase velocity plotted against the dimensionless wavenumber φ at different Courant numbers. Solid curves correspond to the Iserles scheme, while dashed ones correspond to the BiC4-CN scheme.

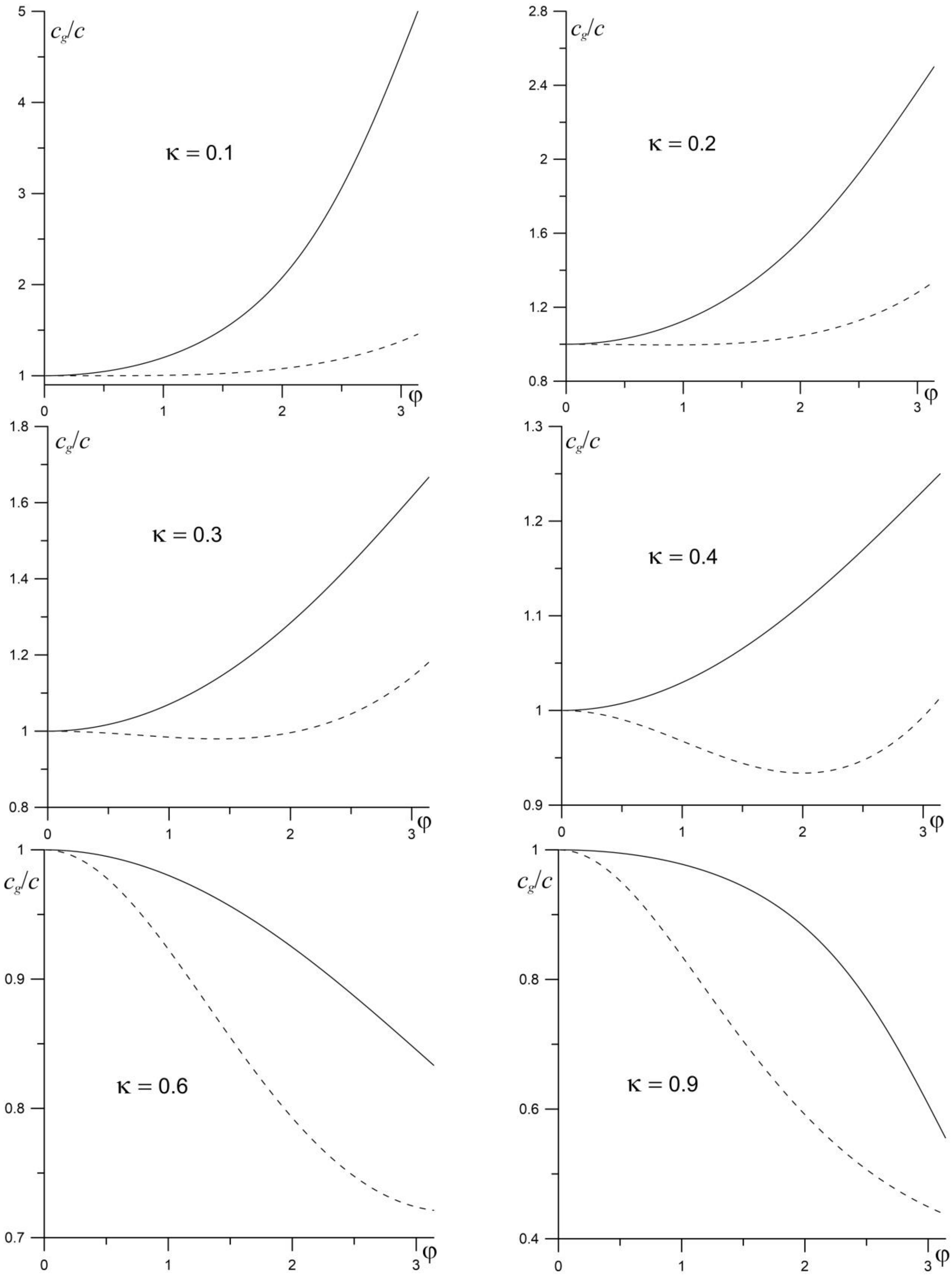

Fig. 10. Numerical group velocity plotted against the dimensionless wavenumber φ at different Courant numbers. Solid curves correspond to the Iserles scheme, while dashed ones correspond to the BiC4-CN scheme.

References

1. Colonius T., Lele S.K. Computational aeroacoustics: progress on nonlinear problems of sound generation // Prog. Aerosp. Sci. 2004. V. 40. P. 345–416.
2. Ekaterinaris J.A. High-order accurate, low numerical diffusion methods for aerodynamics // Prog. Aerosp. Sci. 2005. V. 41. P. 192–300.
3. Kurbatskii K.A., Mankbadi R.R. Review of computational aeroacoustics algorithms // Int. J. Comput. Fluid Dyn. 2004. V. 18. P. 533-546.
4. Bogey C., Bailly C. A family of low dispersive and low dissipative explicit schemes for flow and noise computations // J. Comput. Phys. 2004. V. 194. P. 194–214.
5. Xu D., Deng X., Chen Y., Wang G., Dong Y. Effect of nonuniform grids on high-order finite difference method // Adv. Appl. Math. Mech. 2017. V.9, No.4. P. 1012-1034.
6. Rogov B.V., Mikhailovskaya M.N. Monotone high-order accurate compact scheme for quasilinear hyperbolic equations // Dokl. Math. 2011. V. 84. P. 747-752.
7. Hairer E., Wanner G. Solving Ordinary Differential Equations II: Stiff and Differential-Algebraic Problems. Berlin: Springer-Verlag, 1996.
8. Mikhailovskaya M.N., Rogov B.V. Monotone compact running schemes for systems of hyperbolic equations // Comput. Math. Math. Phys. 2012. V. 52, No. 4. P. 578–600.
9. Rogov B.V. High-order accurate monotone compact running scheme for multidimensional hyperbolic equations // Comput. Math. Math. Phys. 2013. V. 53, No. 2. P. 205–214.
10. Chikitkin A.V., Rogov B.V., Utyuzhnikov S.V. High-order accurate monotone compact running scheme for multidimensional hyperbolic equations // Appl. Numer. Math. 2015. V. 93. P. 150–163.
11. Rogov B.V., Bragin M.D. On spectral-like resolution properties of fourth-order accurate symmetric bicompact schemes // Dokl. Math. 2017. V. 96, No. 1. P. 339–343.
12. Liu X., Zhang S., Zhang H., Shu C.-W. A new class of central compact schemes with spectral-like resolution I: Linear schemes // J. Comput. Phys. 2013. V. 248. P. 235–256.
13. Chikitkin A.V., Rogov B.V. A sixth-order bicompact scheme with spectral-like resolution for hyperbolic equations // Dokl. Math. 2017. V. 96, No. 2. P. 480-485.
14. Chikitkin A.V., Rogov B.V. Family of symmetric bicompact schemes with spectral resolution property for hyperbolic equations // Keldysh Institute Preprints. 2018. No. 144. 27 p. doi:10.20948/prepr-2018-144-e
URL: http://library.keldysh.ru/preprint.asp?id=2018-144&lg=e
15. Chikitkin A.V., Rogov B.V. Optimized symmetric bicompact scheme of the sixth order of approximation with low dispersion for hyperbolic equations // Dokl. Math. 2018. V. 97, No. 1. P. 90–94.

16. Zingg D.W. Comparison of high-accuracy finite difference methods for linear wave propagation // SIAM J. Sci. Comput. 2000. V. 22, No. 2. P. 476–502.
17. Lele S.K. Compact Finite Difference Schemes with Spectral-like Resolution // J. Comput. Phys. 1992. V. 103. P. 16-42.
18. Trefethen L.N. Group velocity in finite difference schemes // SIAM Rev. 1982. V. 24, No. 2. P. 113–136.
19. Sengupta T.K., Dipankar A., Sagaut P. Error dynamics: beyond von Neumann analysis // J. Comput. Phys. 2007. V. 226, No. 2. P. 1211–1218.
20. Sengupta T.K. High accuracy computing methods: fluid flows and wave phenomena. Delhi: Cambridge University Press, 2013.
21. Vichnevetsky R., Bowles J.B. Fourier analysis of numerical approximations of hyperbolic equations. Philadelphia: SIAM, 1982.
22. Trefethen L.N. Finite difference and spectral methods for ordinary and partial differential equations, unpublished text, 1996; freely available online http://people.maths.ox.ac.uk/trefethen/pdetext.html.
23. Hirsch C. Numerical computation of internal and external flows, Vol. 1: Fundamentals of Numerical Discretization. Chichester: John Wiley & Sons, 2001.
24. Iserles A. Generalized leapfrog methods // IMA J. Numer. Anal. 1986. V. 6, No. 3. P. 381-392.
25. Goloviznin V.M., Karabasov S.A., Kozubskaya T.K., Maksimov N.V. CABARET scheme for the numerical solution of aeroacoustics problems: generalization to linearized one-dimensional Euler equations // Comput. Math. Math. Phys. 2009. V. 49, No. 12. P. 2168–2182.
26. Goloviznin V.M., Zaytsev M.A., Karabasov S.A., Korotkin I.A. Novel algorithms of computational hydrodynamics for multicore computing. Moscow: Lomonosov Moscow State University, 2013.

Contents